

Receptor-Level Proximity and Fastening of Ligands Modulates Stem Cell Differentiation

Gunhyu Bae, Myeong Soo Kim, Ramar Thangam, Thomas Myeongseok Koo, Woo Young Jang, Jinho Yoon, Seong-Beom Han, Letao Yang, Seong Yeol Kim, Nayeon Kang, Sunhong Min, Hyunsik Hong, Hong En Fu, Min Jun Ko, Dong-Hwee Kim, Woong Kyo Jeong, Dong-Hyun Kim, Tae-Hyung Kim, Jeong-Woo Choi, Ki-Bum Lee, Ramasamy Paulmurugan, Yangzhi Zhu, Han-Jun Kim, Junmin Lee, Jong Seung Kim, Ali Khademhosseini, Young Keun Kim,* and Heemin Kang*

Cellular adhesion is regulated by the binding of 10 nm sized integrin to Arg-Gly-Asp (RGD) ligands present in extracellular matrix proteins. In this study, seed-mediated growth of gold nanoparticles (AuNPs) on the surface of iron oxide (Fe_3O_4) nanotemplates is employed to tune the diameter and interdistance of RGD-bearing AuNPs at the receptor-level. The Fe_3O_4 nanotemplates decorated with RGD-bearing AuNPs arranged in various RGD diameters and interdistances at the receptor-levels are flexibly fastened to a substrate. Similar to fully connected RGDs, subreceptor-level-gapped (quasicontinuous) RGDs activate integrin binding with the adjacent RGDs, which stimulates focal adhesion, mechanosensing, and differentiation of stem cells. This stimulation of stem cells is hindered when the RGD interdistance increases above the receptor-level gap. However, this stimulation is partially effective when the RGD diameter also increases far above the receptor-level gap. Strikingly, magnetically attracted fastening of the RGDs toward the substrate via polymer linker tightening fully stimulates adhesion and differentiation of stem cells in a reversible manner, both in vitro and in vivo. Various RGD diameter and interdistance on Fe_3O_4 nanotemplates can further elucidate the dynamic receptor-level RGD proximity-regulated stem cell differentiation that govern tissue repair.

1. Introduction

In the native microenvironment, cells are regulated via dynamic interactions with the extracellular matrix (ECM) proteins such as collagen, laminin, and fibronectin (FN) that include Arg-Gly-Asp (RGD) tripeptide motifs within their polypeptide chains.^[1] Collagen is composed of triple-helix polypeptide chains that are ≈ 1.6 nm in diameter and 300 nm in length.^[2] Laminin, composed of rod-like arms that are 2 nm in diameter and terminated with globular units with a diameter of 5–7 nm, contains RGD motif within the α -polypeptide chains.^[3] FN exhibiting modular structures with a length of 16 nm and a width of 9 nm carries RGD loop on the III₁₀ module. Integrin binding to the FN is facilitated or prevented when they are in nonstretched or stretched state, respectively.^[4] Therefore, cell adhesion

G. Bae, R. Thangam, T. M. Koo, S. Y. Kim, N. Kang, S. Min, H. Hong, H. E. Fu, M. J. Ko, Y. K. Kim, H. Kang
Department of Materials Science and Engineering
Korea University
Seoul 02841, Republic of Korea
E-mail: ykim97@korea.ac.kr; heeminkang@korea.ac.kr

M. S. Kim, R. Thangam
Institute for High Technology Materials and Devices
Korea University
Seoul 02841, Republic of Korea


W. Y. Jang, W. K. Jeong
Department of Orthopedic Surgery
Korea University Anam Hospital
Seoul 02841, Republic of Korea

J. Yoon, L. Yang, K.-B. Lee
Department of Chemistry and Chemical Biology
Rutgers University
Piscataway, NJ 08854, USA

J. Yoon, J.-W. Choi
Department of Chemical and Biomolecular Engineering
Sogang University
Seoul 04107, Republic of Korea

S.-B. Han, D.-H. Kim
KU-KIST Graduate School of Converging Science and Technology
Korea University
Seoul 02841, Republic of Korea

D.-H. Kim
Department of Radiology
Feinberg School of Medicine
Northwestern University
Chicago, IL 60208, USA

 The ORCID identification number(s) for the author(s) of this article can be found under <https://doi.org/10.1002/adfm.202200828>.

DOI: 10.1002/adfm.202200828

is actively regulated by cell-adhesive ECM protein units^[5] that exhibit the subintegrin receptor-level proximity (10 nm).^[6] In this regard, we hypothesize that the way cells recognize how the RGDs are interconnected could be modulated by tuning the “diameter” of each RGD and the “interdistance” between the edge of each RGD at the receptor-level proximity by developing novel materials. This receptor-level RGD proximity could dynamically regulate the binding of integrin to neighboring RGDs and thus integrin clustering that triggers stem cell adhesion and differentiation.

Diverse arrangements of cell-adhesive ECM proteins^[7] have been reported to modulate the dynamic formation of integrin-RGD bonds^[8] that regulate the assembly of cytoskeletal F-actin and focal adhesion complexes. This assembly is known to further mediate mechanotransduction pathways and stem cell differentiation.^[9] For instance, arrangements^[10] and tethering^[11] of cell-adhesive ECM proteins are known to modulate the mechanotransduction^[12] and differentiation of stem cells^[13] that mediate tissue repair.^[14] By leveraging these findings, tunable arrangements of RGD sites present in cell-adhesive ECM proteins at the receptor-level proximity can efficiently regulate the integrin ligation that triggers the mechanotransduction and differentiation of stem cells.^[15] Diverse RGD arrangements have been constructed by patterning typical 10 nm sized gold nanoparticles (AuNPs) on a substrate. Both we and other groups have reported tuning of RGD interdistance,^[16] RGD nanogeometry,^[17] RGD micropattern,^[18] RGD ordering/disordering,^[19] local/global RGD density,^[20] RGD clustering,^[21] and RGD sequence^[22] to modulate cell adhesion. In these studies, an interdistance between the adjacent RGD-bearing AuNPs below ≈ 70 nm has been consistently reported to stimulate cell adhesion.^[16,18b,19,20]

In particular, integrin clusters were shown to bridge densely distributed linear RGD sites spaced below 110 nm, which activated cell adhesion.^[23] In previous studies that exploited the lithographical patterning approach,^[16,18b,19,20] constructing RGDs at the receptor-level has not yet been achieved probably owing to the intrinsic repulsion between the neighboring AuNPs.^[24] Therefore, novel approaches are required to overcome this fundamental limit to unravel integrin-RGD interactions. Furthermore, the RGD motif-bearing 3D structure can be emulated by endowing planar RGD arrangements with an ability to be axially shifted, which is similar to the ECM^[25] that dynamically remodels in vivo. Tissue-penetrative stimuli,^[26] such as a magnetic field^[27] can be used to achieve such dynamic remodeling via manipulation of magnetic nanomaterials^[28] that are flexibly grafted to a substrate, which can, in turn, influence the integrin-RGD bond formation on dynamic RGD arrangements. Developing novel materials^[29] that possess the tunability of RGD diameter and interdistance at the receptor-level RGD proximity along with dynamic property can help to decipher the complexity of the cell-ECM interplay.^[30]

In this study, we synthesized AuNPs of desired size, then grafted them to the iron oxide (Fe₃O₄) nanotemplate surface. Depending on the required group conditions (RGD diameter and RGD interdistance), AuNPs were subjected to seed-mediated growth (before or after Fe₃O₄ nanotemplate grafting) (**Scheme 1**). For sensitive manipulation of integrin clustering at the receptor-level RGD proximity, RGD arrangements were densely localized on the Fe₃O₄ nanotemplates sparsely distributed on substrate to maintain global RGD density similar to that shown in previous studies.^[16,18b,19,20] Using this strategy, we attained tunable RGD-bearing AuNPs (RGD-AuNPs) with varying diameter (designated as “X” in nm) and edge-to-edge RGD interdistance (designated as “Y” in nm) with their tuned arrangements noted as (X, Y) on Fe₃O₄ nanotemplates. It is fundamentally challenging to synthesize and graft AuNPs with their interdistance below 4 nm to the nanotemplate owing to the inherent repulsion between the AuNPs.^[24] In particular, we attained “Small-sized RGD” referred to as “S” group that exhibit subreceptor-level RGD interdistance between the two edges of adjacent RGD-grafted AuNPs via our seed-mediated growth approach using the nanotemplate, thus overcoming the fundamental limit restraint.

Strikingly, this RGD diameter and interdistance lie within the receptor-level RGD proximity, which is recognized by the cells as being connected, and thus a continuous RGD layer (i.e., quasicomnected). This enables integrins to bind to the adjacent RGD-grafted AuNPs to trigger saturated integrin clustering in stem cells, leading to the activation of focal adhesion, mechanotransduction, and differentiation, both in vitro and in vivo. This level of stem cell activation was comparable to that of the completely connected RGD-bearing AuNPs in a “Shell, zero distance” (200 nm in diameter) with 0 nm edge-to-edge RGD interdistance on a Fe₃O₄ nanotemplate. The RGD diameters and edge-to-edge RGD interdistances were tuned at the receptor-level RGD proximity without modulating the global RGD density in three groups: “Small-sized RGD” referred to as “S,” “Medium-sized RGD” referred to as “M” group, and “Large-sized RGD” referred to as “L” group. When the RGD interdistance was increased from subreceptor-level gap of the “S” group to receptor-level gap

T.-H. Kim
School of Integrative Engineering
Chung-Ang University
Seoul 06974, Republic of Korea

R. Paulmurugan
Department of Radiology
Molecular Imaging Program at Stanford
Stanford University School of Medicine
Stanford University
Palo Alto, CA 94304, USA

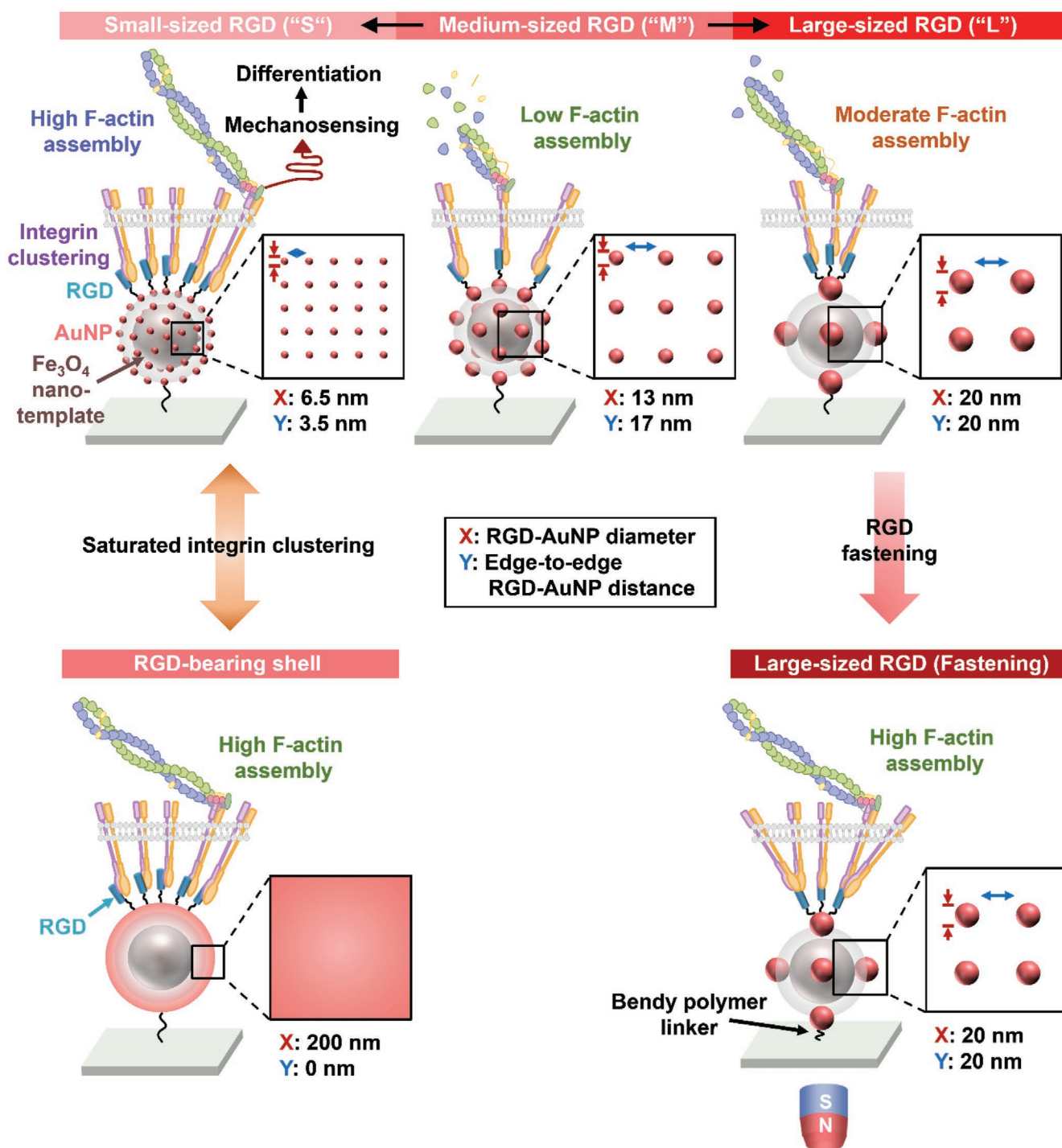
R. Paulmurugan
Department of Radiology
Canary Center at Stanford for Cancer Early Detection
Stanford University School of Medicine
Stanford University
Palo Alto, CA 94304, USA

Y. Zhu, H.-J. Kim, A. Khademhosseini
Terasaki Institute for Biomedical Innovation
Los Angeles, CA 90064, USA

J. Lee
Department of Materials Science and Engineering
Pohang University of Science and Technology (POSTECH)
Pohang 37673, Republic of Korea

J. S. Kim
Department of Chemistry
Korea University
Seoul 02841, Republic of Korea

H. Kang
Department of Biomicrosystem Technology
Korea University
Seoul 02841, Republic of Korea



Scheme 1. A schematic illustration of the study design. Tuning of receptor-level RGD proximity for the "Small"-, "Medium"-, and "Large"-sized RGD-AuNP groups with the following notations: (RGD diameter, edge-to-edge RGD distance). Both the RGD interdistance of the quasicomposed "S" group and the completely connected RGD of the Au "Shell" (200, 0) group stimulate integrin binding across the adjacent RGD sites to trigger saturated integrin clustering, focal adhesion, mechanotransduction, and differentiation of stem cells to a similar degree, both in vitro and in vivo. Increasing the RGD interdistance from the "S" group to the unconnected "M" group significantly hinders integrin clustering and stem cell adhesion. Increasing the RGD diameter from the "S" group to the "L" group enabled partial integrin binding to the neighboring RGD sites, thereby slightly promoting integrin clustering and stem cell adhesion. Magnetic attraction applied to the "L" group fastened the RGD-bearing AuNPs toward the substrate via tightening of the flexible polymer linker between the Fe₃O₄ nanotemplates and the substrate. Such magnetic fastening facilitated firm integrin binding to the RGD sites, thereby stimulating integrin clustering and stem cell adhesion and differentiation in vivo to a comparable level to the quasicomposed "S" group.

of the “M” group, stem cells recognized the RGD sites as unconnected. Consequently, multiple integrins could not connect to the neighboring RGD sites and cluster, thereby hindering the adhesion formation, mechanotransduction, and differentiation of stem cells. Control experiments of independently tuning the RGD interdistance for the “S, small distance” and “S, large distance” groups, respectively, corroborated this trend.

However, when the RGD diameter was increased from the “S” group and the “M” group to the “L” group, multiple integrins could bind to each 20 nm RGD site and partially to neighboring ones, thereby slightly promoting the adhesion formation, mechanotransduction, and differentiation of stem cells. Interestingly, although the cells recognize 20 nm spaced RGDs as unconnected in the “L” group, fastening the RGD arrangements (grafted to the substrate via a bendy polymer linker) by magnetically attracting the Fe₃O₄ nanotemplates toward the substrate surface helped integrin to firmly bind to the neighboring RGD sites, thereby significantly stimulating the adhesion formation and differentiation to a comparable degree to those demonstrated by the “S” (quasiconnected RGD) group. This comparison of dynamic manipulation^[26g] of unconnected RGD arrangements versus static receptor-level RGD arrangements is clearly different from our recent studies of magnetically manipulating the RGD pitch in nanocoils^[31] and RGD sliding^[32] as well as 1D fiber-mimicking linear RGD patterns.^[23] Herein, we present the modulation of receptor-level RGD proximity that regulates stem cell differentiation for advancing dynamic regenerative therapies.^[33]

2. Results and Discussion

2.1. Tuning of Receptor-Level RGD Proximity

To develop various RGD diameter and interdistance at the receptor-level, we prepared diverse RGD-bearing AuNP arrangements by grafting AuNPs onto the Fe₃O₄ nanotemplate surface, and then mediated seed-mediated growth of the AuNPs. The crystalline phase of the Fe₃O₄ nanotemplates was identified via X-ray diffraction (XRD) analysis, while the reversible magnetic characteristics of Fe₃O₄ nanotemplates with high saturation magnetization of 73.8 emu g⁻¹ and nearly zero coercivity were verified using vibrating sample magnetometer (VSM) analysis (Figures S1 and S2, Supporting Information). To graft the AuNPs to the surface of Fe₃O₄ nanotemplates via Au-amine bonding, a uniform amino-SiO₂ layer was coated on the latter, which increased the hydrodynamic diameter from 174 ± 18 to 213 ± 22 nm, as verified through transmission electron microscopy (TEM) and dynamic light scattering (DLS) analysis (Figure S3a,b, Supporting Information).

By modulating the Au³⁺ concentration, reducing agents, and reaction temperature, AuNP seeds of tunable diameters (3.5 vs 13 nm) were directly synthesized, whereas 20 nm diameter AuNPs were prepared via the seed-mediated growth of 13 nm AuNPs. Through this procedure, homogeneous spherical AuNPs with various diameters were synthesized (12.4 ± 1.0, 23.2 ± 1.1, 31.6 ± 1.0, and 52.7 ± 4.3 nm) as shown in the TEM images, which exhibited similar absorption peaks at 520 nm as verified by UV–vis absorbance spectrometry (Figure S4a–c,

Supporting Information). To prepare the “S” RGD-bearing AuNP arrangement, 3.5 nm AuNPs were grafted onto the surface of Fe₃O₄ nanotemplate, stabilized with polyvinylpyrrolidone (PVP), and then subjected to nanotemplate-mediated growth of the 3.5 nm AuNP seeds. By controlling the number of repetitions of supplying low Au³⁺ ion amounts to prevent Au self-nucleation, the diameters of compact assembly of in situ-grown AuNPs were tuned as 3.5 ± 0.6, 6.5 ± 0.5, 8.7 ± 0.5, and 10.7 ± 1.1 nm, as shown in the TEM images, which exhibited redshift of the UV–vis absorption peaks with increasing AuNP diameter (Figure 1a; and Figure S5a–c, Supporting Information).

High angle annular dark field-scanning TEM (HAADF-STEM) and energy-dispersive X-ray spectroscopy (EDS) mapping verified the even distribution of the AuNPs (depicted by brighter shade and green-colored Au element) with uniform diameters and interdistances on the Fe₃O₄ nanotemplate (described by darker shade and purple-colored Fe element) in the “S,” “M,” and “L” groups (Figure 1b). The HAADF-STEM images revealed an even distribution of AuNPs on each Fe₃O₄ nanotemplate with AuNP diameters of 6.4 ± 0.2, 12.9 ± 0.5, and 19.3 ± 0.9 nm; AuNP interdistances of 3.6 ± 0.2, 17.4 ± 1.1, and 20.1 ± 1.4 nm; and the number of AuNPs per Fe₃O₄ nanotemplate of 484.8 ± 10.1, 146.8 ± 4.7, and 55.4 ± 2.9 nm for the “S,” “M,” and “L” groups, respectively (Figure 1c). Variation in the total surface area of the AuNPs per Fe₃O₄ nanotemplate (59 913–64 936 nm²) was not statistically significant, thereby providing proof of the successful tuning of RGD-bearing AuNP diameter and interdistance independently from the RGD density for all three groups. High resolution-scanning TEM (HR-STEM) images demonstrated the atomic arrangements of the crystalline phase of Fe₃O₄ and AuNPs, which were used to confirm the average unit cell lattice parameter and the average lattice spacing, respectively (Figure 1d). Meanwhile, the “S,” “M,” and “L” groups exhibited UV–vis absorption peaks corresponding to the AuNPs (at 520 nm) and Fe₃O₄ nanotemplates (at 408 nm) with similar hydrodynamic diameters (Figure S6a,b, Supporting Information). XRD patterns of “S,” “M,” and “L” groups confirmed the copresence of Fe₃O₄ and Au, while the results of the VSM analysis proved their magnetically reversible characteristics (Figures S7 and S8, Supporting Information).

To graft the RGD arrangements on the substrate surface, we coated AuNP arrangements on the Fe₃O₄ nanotemplates (“S,” “M,” and “L” groups) with flexible poly(ethylene glycol) (PEG, M_w: 5000 Da) linker (carboxymethyl-PEG-thiol) via gold-thiol bonding, which were then grafted to an amine-activated substrate via the N-ethyl-N’-(3-(dimethylaminopropyl) carbodiimide/N-hydroxysuccinimide (EDC/NHS) reaction (Scheme 2). Before AuNP arrangement grafting to the substrate, reaction time of AuNP seed-mediated growth was precisely modulated to tune the diameter and interdistance of the RGD-bearing AuNP arrangements (independently from the Fe₃O₄ nanotemplate and global RGD densities) and enable the magnetic fastening control of the RGD-bearing AuNP arrangements to emulate the 3D dynamics of the ECM. To mediate the RGD arrangement-specific integrin binding and clustering of stem cells, substrate surfaces not coated with RGD arrangements and residue amine functional groups on Fe₃O₄ nanotemplate surfaces were blocked using methoxy group-presenting PEG (Scheme 2). The carboxyl group activated PEGylated

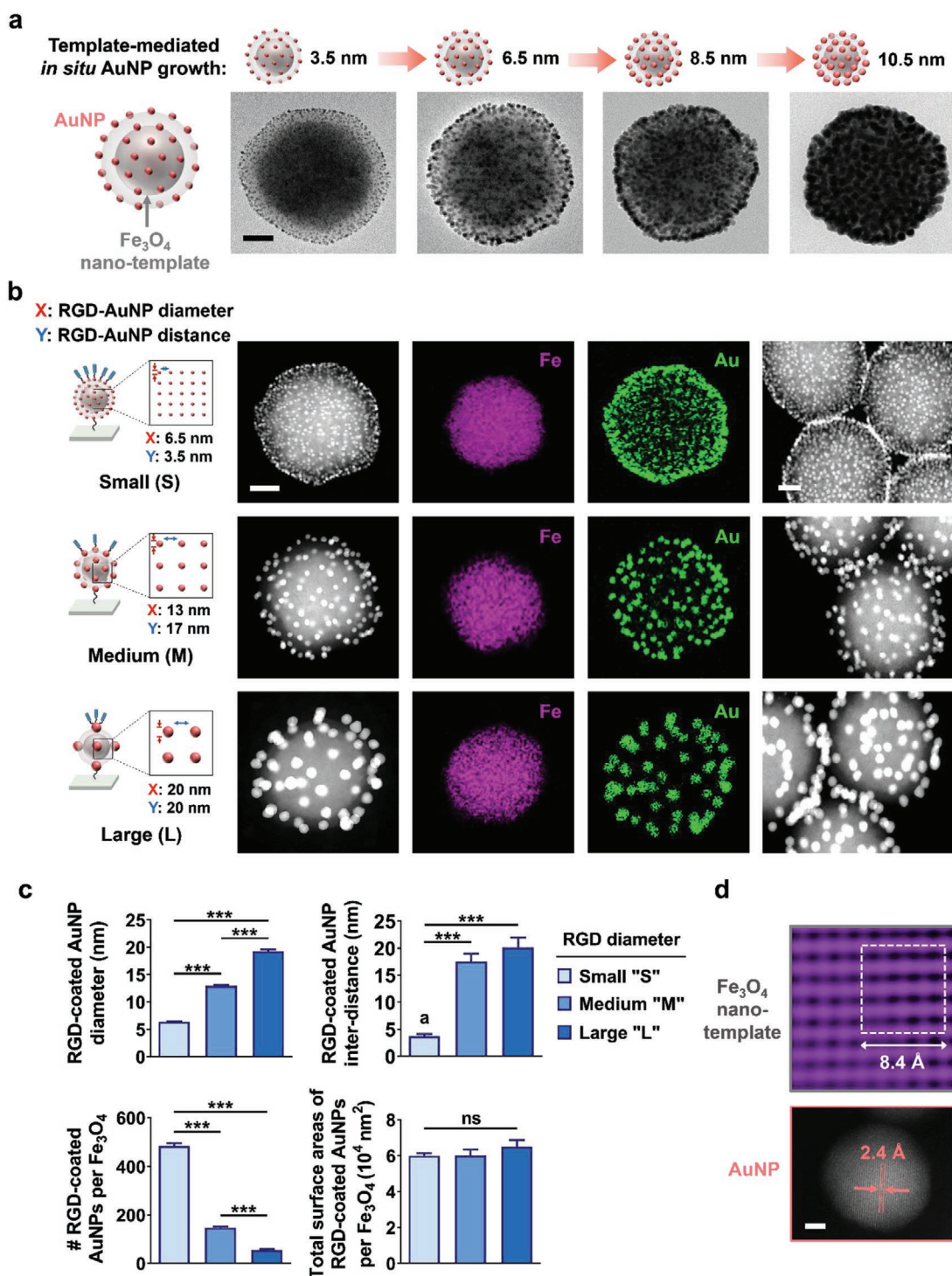
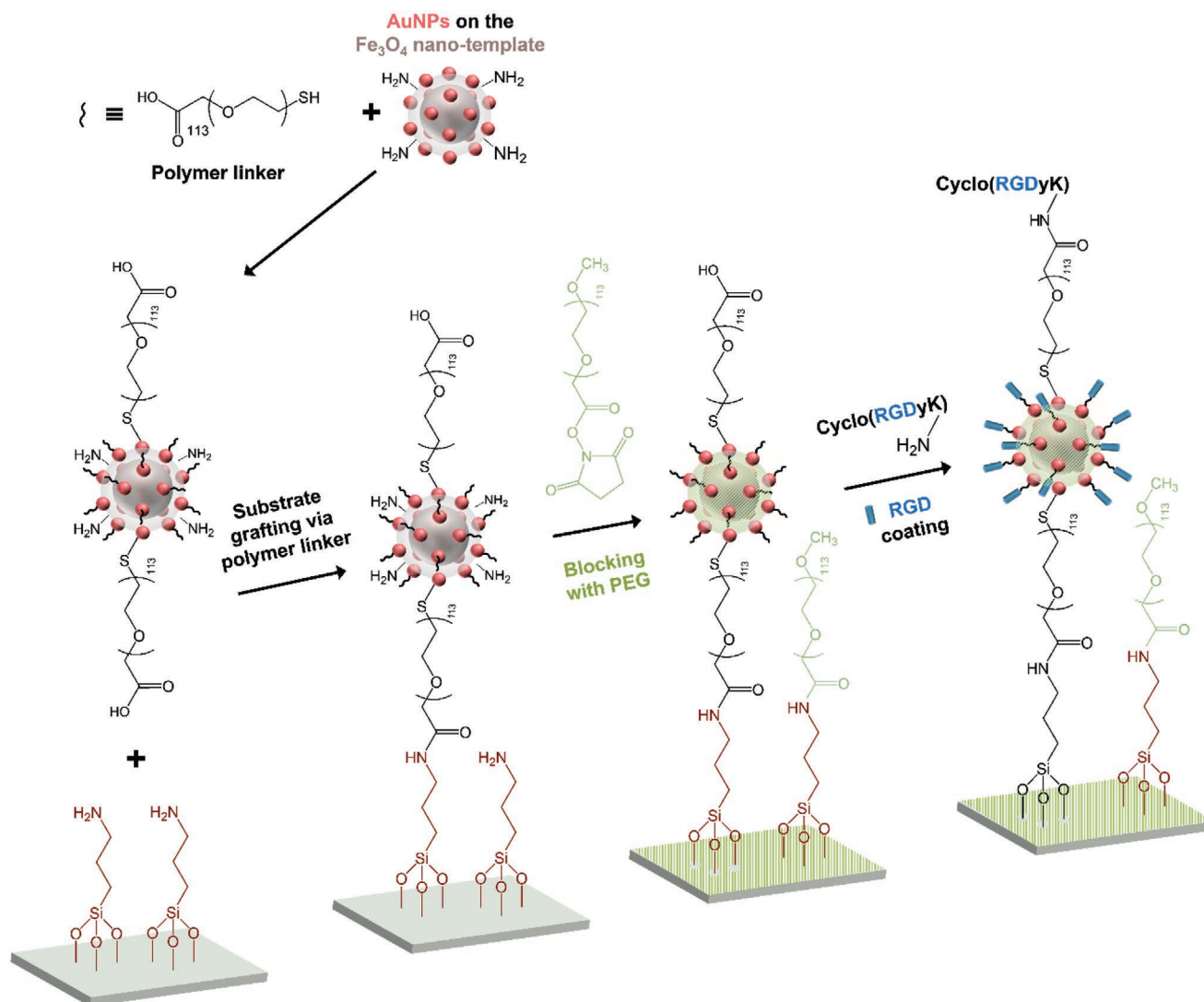


Figure 1. Tuning of receptor-level RGD proximity. a) Transmission electron microscopy (TEM) images of *in situ*-grown AuNPs with controlled diameters on the Fe₃O₄ nanotemplates. Scale bar: 50 nm. b) High angle annular dark field-scanning TEM (HAADF-STEM) images at high and low magnification and subsequent energy-dispersive spectroscopy (EDS) mapping (the Fe element from the Fe₃O₄ nanotemplate and the Au element from the AuNPs) of the tunable RGD-bearing AuNP nanoarrangements on Fe₃O₄ nanotemplates (independent of the RGD density) of “Small (S)”, “Medium (M)”, and “Large (L)”-sized RGD groups with the following notations: (RGD-bearing AuNP diameter, edge-to-edge RGD interdistance). Scale bars: 50 nm. c) Following quantifications of the RGD diameter and interdistance, the number of RGD-bearing AuNPs per Fe₃O₄ nanotemplate, and the total surface area of the RGD-bearing AuNPs per Fe₃O₄ nano-template. d) High resolution-STEM (HR-STEM) atomic-level images of Fe₃O₄ nanotemplate with the average unit cell lattice parameter and AuNPs with the average lattice spacing. Scale bar: 2 nm. Data are shown as the mean ± standard error ($n = 10$). Asterisks were assigned to p values with statistical significances for multiple groups compared by one-way analysis of variance with Tukey–Kramer post-hoc tests (***: $p < 0.001$). ns indicates that there are no statistically significant differences. The experiments in a–d) were repeated three times.



Scheme 2. A schematic illustration of grafting Fe_3O_4 nanotemplates to a substrate, which presents tunable RGD diameter and interdistance at the receptor-level. Serial chemical reactions in the PEGylation, substrate coupling, PEG blocking, and RGD coating are illustrated, which enabled the substrate grafting of the Fe_3O_4 nanotemplates with tunable RGD diameter and interdistance without changing the Fe_3O_4 nanotemplate density. PEG blocking allowed the RGD arrangement-specific stem cell regulation. This configuration enabled the remote manipulation of RGD fastening via the bending of PEG linker by applying an external magnetic field.

AuNP arrangements were then reacted with the amine groups of cyclic RGD peptides bearing lysine residues. Sequential chemical reactions while preparing the RGD-bearing AuNP arrangements (the “S,” “M,” and “L” groups) were confirmed by using Fourier transform infrared (FTIR) spectra after PVP stabilization, PEG grafting, and RGD peptide coating (Figure S9, Supporting Information). The “S,” “M,” and “L” RGD-bearing AuNP arrangements on Fe_3O_4 nanotemplates were confirmed to be evenly distributed via field emission-scanning electron microscopy (FE-SEM) images, which exhibited invariant Fe_3O_4 nanotemplate density between 1.13 and 1.26 per μm^2 . Compared to the previously reported RGD-bearing AuNP densities,^[16,18b,19,20] the Fe_3O_4 nanotemplate density in our study was significantly lower, whereas the density of the AuNPs on each Fe_3O_4 nanotemplate was considerably higher, yielding similar substrate-grafted global RGD densities between the groups ranging from 73 650 to 75 610 $\text{nm}^2 \mu\text{m}^{-2}$. The

substrate-grafted global RGD densities were calculated by multiplying the Fe_3O_4 nanotemplate density by the total surface area of AuNPs per Fe_3O_4 nanotemplate (Figure S10a,b, Supporting Information). This global RGD density was optimized for effective stem cell regulation in our study, the details of which are given later. Moreover, the substrates bearing tunable RGD arrangements grafted on Fe_3O_4 nanotemplates exhibited no cytotoxicity, thereby suggesting the potential biomedical applicability of our developed materials for regulating stem cell-based tissue repair (Figure S11a,b, Supporting Information).

2.2. Receptor-Level RGD Proximity Alters Integrin Clustering-Aided Stem Cell Adhesion and Differentiation

We next pondered how tuning the RGD diameter and interdistance at constant global RGD density could regulate

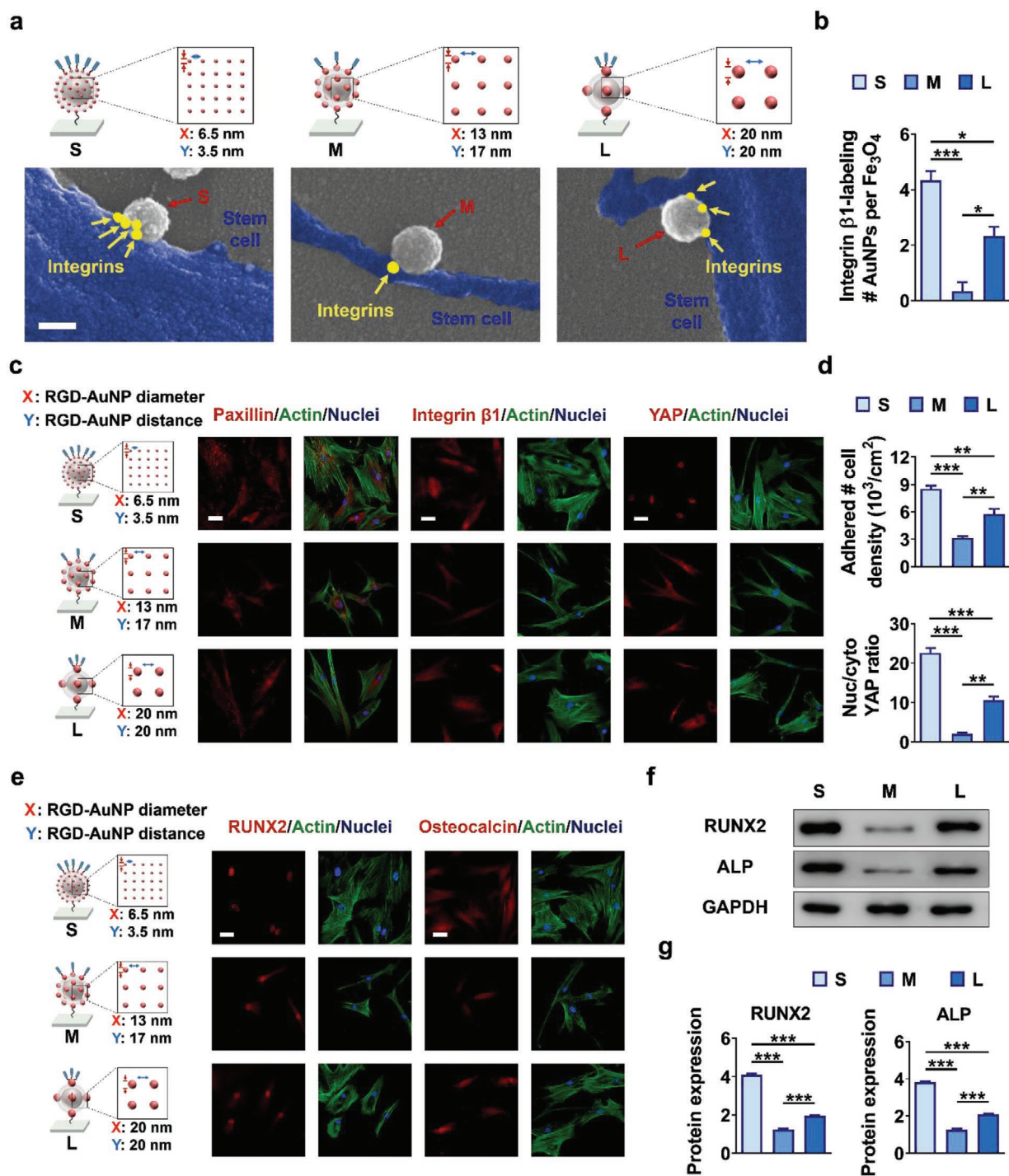


Figure 2. RGD interdistance is dominant over RGD diameter in stem cell regulation independently from the global RGD density. a) Field emission-scanning electron microscopy (FE-SEM) images of gold immuno-labeled integrin $\beta 1$ clustering (yellow arrows) in adherent stem cell (blue) recruited to tunable RGD-AuNP arrangements (red arrows) after 24 h of culturing in the “S,” “M,” and “L” groups with the following notations: (RGD diameter, edge-to-edge RGD distance). Scale bar: 200 nm. b) Following quantification for the number of integrin $\beta 1$ -labeled AuNPs per Fe_3O_4 nanotemplate. c) Confocal microscopy images after immunofluorescence staining for paxillin, integrin $\beta 1$, and YAP costained with F-actin/nuclei of stem cells after 48 h of culturing in growth medium on the “S,” “M,” or “L” groups. Scale bars: 50 μm . d) Following quantifications of the number of adhered stem cells and nucleus/cytoplasm YAP ratio. e) Confocal microscopy images after immunofluorescence staining for osteogenic differentiation markers of RUNX2 and osteocalcin costained with F-actin/nuclei, Scale bars: 50 μm . f) Western blotting analysis and g) following quantification of RUNX2 and ALP protein expressions (normalized to GAPDH) of stem cells after 4 d of culturing in osteogenic induction medium on the “S,” “M,” and “L” groups. Data are shown as the mean \pm standard error ($n = 10$). Asterisks were assigned to p values with statistical significances for multiple groups compared by one-way analysis of variance with Tukey–Kramer post-hoc tests (*: $p < 0.05$; **: $p < 0.01$; ***: $p < 0.001$). The experiments in a–g) were repeated three times.

integrin binding and clustering of human mesenchymal stem cells (hMSCs). The “S” group with RGD diameter and interdistance within the receptor-level proximity was prepared to examine whether integrin could bind to the adjacent RGDs to facilitate saturated integrin clustering. The “M” group with RGD diameter and interdistance slightly above the receptor-level was prepared to probe whether the integrin could bind to the unconnected adjacent RGD and cluster. The “L” group nm was prepared to evaluate the multiple integrins binding to each RGD site to partially connect the adjacent RGDs as opposed to integrin binding to each RGD site in the “S” and “M” groups. Incubation of the “S,” “M,” and “L” groups with integrin $\beta 1$ revealed that integrin clustering was substantially high, negligible, and low, respectively, thereby supporting our hypothesis (Figure S12a,b, Supporting Information). This trend of facilitated integrin $\beta 1$ clustering to the closely spaced RGD sites was corroborated by nanolevel gold-immunolabeled single-cell-level FE-SEM imaging, which examined the directly recruited integrin $\beta 1$ of stem cells (via 40 nm AuNPs) to the tunable RGD arrangements, as well as immunofluorescence staining that examined the integrin $\beta 1$ expression in adhered stem cells (Figure 2a–c). Immunofluorescence-stained images of paxillin (a focal adhesion adaptor), F-actin, and YAP (a mechanotransducer) in stem cells after 48 h of plating showed a considerable increase in stem cell adhesion and the spread of F-actin assembly in the “S” group, which was less evident in the “M” and “L” groups (Figure 2c; and Figure S13a, Supporting Information). Moreover, quantification of the number of adhered stem cells, spread cell area, number of focal adhesions, and YAP nucleus/cytoplasm ratio all demonstrated homogeneous enhancement behavior in the order of “S,” “L,” and “M” groups (Figure 2d; and Figure S13b, Supporting Information). This efficient receptor-level RGD proximity-specific stem cell regulation was authenticated via control experiments where the RGDs were not grafted to the AuNPs or the RADs (a scrambled RGD sequence) were grafted to the AuNPs instead of RGD. Immunofluorescence-stained images revealed minimal adhesion of stem cells without considerable differences between these groups (Figures S14a,b and S15a,b, Supporting Information). Taken together, these findings support our hypothesis that integrin clustering-assisted stem cell adhesion and mechanotransduction are highly facilitated via integrin binding to the subreceptor-level gapped RGDs in the “S” group, slightly promoted via multiple integrins binding to each 20 nm RGD site and partially to the neighboring RGD sites in the “L” group, and restrained via integrin binding to each 13 nm RGD site that cannot bind to neighboring RGD sites in the “M” group. Accordingly, we can deduce that the RGD interdistance and diameter are primary and secondary factors that regulate stem cells, respectively.

The integrin clustering in stem cells activates focal adhesion-mediated mechanotransduction signaling pathways that facilitate their fates, such as osteoblastic differentiation. Therefore, we investigated this in regards to the receptor-level RGD proximity-dependent regulation.^[15a,34] After 4 d of culturing stem cells in osteogenic induction medium, immunofluorescence-stained imaging along with western blotting analysis proved that the “S” group facilitated prominent expression of both the early osteogenic markers (pronounced nuclear

translocation in RUNX2 and protein expression of RUNX2 and ALP) and the late osteogenic marker (osteocalcin), which was followed by the order of the “L” and then the “M” groups (Figure 2e–g; and Figure S16a,b, Supporting Information). These results suggest that the shorter interdistance between the RGDs in the “S” group successfully promotes integrin clustering and mechanotransduction signaling that lead to the differentiation of stem cells.

2.3. Quasiconnected-RGD-Modulate Stem Cell Regulation by Independently Tuning the RGD Interdistance

Next, we considered how the independent tuning of RGD interdistance effect stem cell regulation through comparing the groups of “S, large distance” versus “S, small distance” versus continuous Au “Shell, zero distance,” modulated by controlling the Au³⁺ concentration and reducing agents. The HAADF-STEM images of the “S, large distance,” “S, small distance,” and “Shell, zero distance” groups confirmed the even distribution of the AuNPs on each Fe₃O₄ nanotemplate (Figure 3a; and Figure S17a, Supporting Information). The “S, large distance” and “S, small distance” groups yielded similar AuNP diameters of 6.5 and 6.6 nm with significantly different AuNP interdistances of 18.6 ± 0.6 and 3.4 ± 0.3 nm, respectively (Figure S17b, Supporting Information). The FE-SEM images showed evenly distributed Fe₃O₄ nanotemplates for the “S, large distance,” “S, small distance,” and “Shell, zero distance” groups with constant Fe₃O₄ nanotemplate densities but significantly different substrate-grafted global RGD density of $19\,500 \pm 245$ nm² μm^{-2} , $79\,000 \pm 1050$ nm² μm^{-2} , and $193\,000 \pm 8760$ nm² μm^{-2} , respectively (Figure S18a,b, Supporting Information).

Even though the global RGD density of the “Shell, zero distance” group is significantly higher than that of the “S, small distance” group, immunofluorescence-stained images along with the corresponding quantification analysis showed similar adhered cell number, spread cell area, number of focal adhesions, and nucleus/cytoplasm YAP and RUNX2 ratios with no statistically significant differences between the two groups, which were all remarkably low in the “S, large distance” group (Figure 3a–d; and Figure S18c, Supporting Information). These findings demonstrate that despite lower global density, the RGD inter-distance of 3.5 nm is recognized by the cells as a continuous RGD layer, analogous to the connected RGD sites in the Au “Shell, zero distance” group. Thus, integrin of 10 nm in size can bind to the neighboring subreceptor-level-spaced RGD sites, thereby yielding saturated (maximal) integrin clustering that leads to pronounced stem cell adhesion. Increasing the RGD interdistance above the threshold of 17 nm (slightly exceeding the size of FN and integrin) in the “S, large distance” group results in unconnected RGDs such that integrin cannot bind to the widely spaced neighboring RGDs, which restrains integrin clustering and consequential stem cell adhesion and differentiation. When exceeding this threshold, increasing the RGD diameter to 13 nm in the “M” group despite its identical RGD density to the “S” group nullifies the promotion of integrin clustering, and stem cell adhesion and differentiation. This suggests that each 13 nm RGD site accommodates the binding of integrin but not clustering across the neighboring

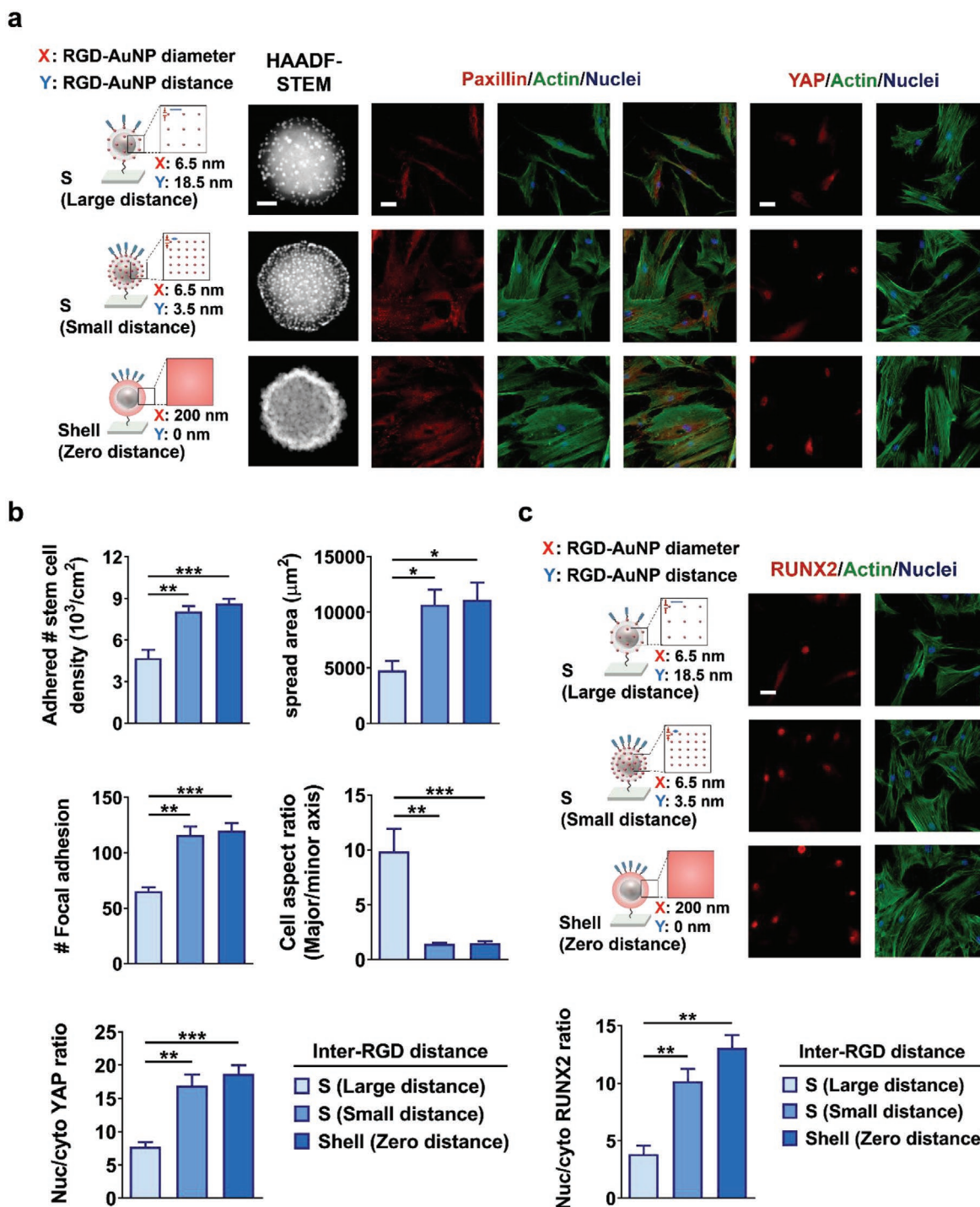


Figure 3. Quasiconnected RGD arrangements stimulate the focal adhesion, mechanotransduction, and differentiation of stem cells comparably to the connected RGDs. a) High angle annular dark field-scanning transmission electron microscopy (HAADF-STEM) images and confocal immunofluorescence staining images for paxillin and YAP, costained with F-actin/nuclei of stem cells after 48 h of culturing in growth medium on the “S, large distance,” “S, small distance,” or “Shell, zero distance” RGD-AuNP arrangements with the following notations: (RGD diameter, edge-to-edge RGD distance). In the RGD-coated Au shell covering an entire surface of each Fe_3O_4 nanotemplate, the diameter of each Fe_3O_4 nanotemplate was calculated as RGD diameter with zero RGD interdistance. b) Following quantification of the number of adhered stem cells, spread cell area, the number of focal adhesions, cell aspect ratio, and nucleus/cytoplasm YAP ratio. c) Confocal microscopy images after immunofluorescence staining for RUNX2 costained with F-actin/nuclei of stem cells along with subsequent quantification of RUNX2 nucleus/cytoplasm ratio after 24 h of culturing in osteogenic induction medium on the identical groups as above. Scale bars: 50 nm for the HAADF-STEM and 50 μm for the confocal immunofluorescence. Data are shown as the mean \pm standard error ($n = 10$). Asterisks were assigned to p values with statistical significances for multiple groups compared by one-way analysis of variance with Tukey–Kramer post-hoc tests (*: $p < 0.05$; **: $p < 0.01$; ***: $p < 0.001$). The experiments in a–c) were repeated three times.

RGD sites. However, when the RGD diameter exceeds 20 nm (in the “L” group), multiple (most likely two) integrins can bind to each RGD site, which thus increases the chance of clustering across the RGD sites, resulting in partial promotion of integrin clustering, and resultant stem cell adhesion and differentiation. To consolidate our findings and solely attribute the differed cellular regulation to the tunable RGD arrangements grafted on Fe₃O₄ nanotemplates (the “S, large distance,” “S, small distance,” “Shell, zero distance,” “M,” and “L” groups), substrate surface wettability, chargeability, and roughness were also analyzed. No statistically significant difference among the groups for such surface characteristics confirmed that there were no potential factors that could have additionally affected cell adhesion (Figure S19a–c, Supporting Information).

In summary, Our nanotemplate-mediated AuNP growth approach offers unlimited tunability of the RGD diameter and interdistance as well as Fe₃O₄ nanotemplate diameter and shape to further unravel the mechanism of integrin clustering on numerous RGD architectures. These findings provide an understanding of the receptor-level RGD interactions on the localized Fe₃O₄ nanotemplates, and are thus different from the majority of studies that have shown the RGD interdistance below 70 nm to stimulate cell adhesion, and integrin clusters to bridge the RGD lines spaced below 110 nm,^[16,18b,19,20,23] which are far greater than the receptor-level RGD proximity level.

2.4. Remote Manipulation of RGD Fastening for Reversible Stem Cell Regulation

We next considered whether the RGD arrangements perceived by the stem cells can be reversibly changed. To this end, the unconnected RGD “L” group was used, with the reason to be explained later on. To magnetically induce reversible RGD fastening [the “L (Fastened)” group] or unfastening [the “L (Unfastened)” group], a permanent magnet was either placed or not placed near the lower side of the substrate, respectively. RGD fastening was achieved through bending while RGD unfastening was achieved through releasing of the polymer linker used to graft the RGD arrangements on Fe₃O₄ nanotemplates to the substrate. Reversible atomic force microscopy (AFM) confirmed axial downward shift of the RGD arrangements in the “L (Fastened)” group (darker contrast, 200.0 ± 13.87 nm) that decreased their height by 10 nm compared to those in the “L (Unfastened)” group (brighter contrast, 211.0 ± 12.64 nm). The reversibility of such magnetic manipulation was confirmed through repeated cycle of fastening, where the height of “L (Fastened)” group (darker contrast, 200.0 ± 5.1 nm) was also decreased by 10 nm compared to the “L (Unfastened)” group (brighter contrast, 210.3 ± 1.2 nm) (Figure S20a,b, Supporting Information).

Immunofluorescence-stained images, western blotting, and corresponding quantification analysis of the adhered number of stem cells, spread cell area, number of focal adhesions, nucleus/cytoplasm YAP and RUNX2 ratio, and RUNX2 and ALP expression consistently revealed significant increases for the “L (Fastened)” group compared to the “L (Unfastened)” group to a comparable degree to which was previously observed in the quasi-connected group (Figures 2c–g, 4a–e; and Figure S20c, Supporting Information). Since the polymer

linker used in this study (molecular weight of 5000 Da) is ≈38 nm long,^[11,35] the 10 nm height change via RGD fastening could help multiple integrins to bind to each 20 nm RGDs and firmly to the “unconnected” neighboring RGDs, which stimulates dynamic stem cell adhesion and differentiation. The “L” group was chosen since it showed the most promoted cell adhesion upon magnetic fastening. Confocal immunofluorescence staining images of magnetically controlled different RGD arrangements grafted on Fe₃O₄ nanotemplate (“S, Unfas,” “S, Fas,” “M, Unfas,” “M, Fas,” “L, Unfas,” and “L, Fas” groups) showed that magnetic fastening of the “S” and the “M” groups were not as effective as the “L” group (Figure S21a,b, Supporting Information).

Real-time confocal microscopy imaging of the “L (Fastened)” group after initial 4 h exhibited high degree of stem cell adhesion. After switching the “L (Fastened)” state to the “L (Unfastened)” state after 4 h, the stem cell adhesion was degraded to the level similar to the unconnected RGD state, thereby proving reversible stem cell adhesion (Movie 1, Supporting Information). This dynamic switching of receptor-level RGD proximity has not been shown in prior studies of magnetically induced RGD pitch modulation^[31] and macrolevel RGD sliding.^[32] We also identified the molecular machinery involved in the receptor-level RGD proximity-regulated focal adhesion that mediates the mechanotransduction of stem cells. Originally, the “S” (quasi-connected) and “L (Fastened)” RGD groups exhibited remarkably high degree of stem cell adhesion and nucleus/cytoplasm YAP ratio (Figures S22 and S23, Supporting Information). When the inhibitors specific to actin polymerization (Cytochalasin D), rho-associated protein kinase (ROCK) (Y27632), and myosin II (Blebbistatin) were added, such high degree of stem cell adhesion and nucleus/cytoplasm YAP ratio significantly decreased, thus proving the involvement of the corresponding molecular machinery.

2.5. In Vivo Receptor-Level RGD Proximity-Modulated Dynamic Regulation of Stem Cell Differentiation

As a proof-of-principle for the receptor-level RGD proximity- and fastening-based dynamic stem cell regulation in vivo, we implanted substrates presenting tunable RGD arrangements grafted on Fe₃O₄ nanotemplates into the subcutaneous pockets of mice. Subsequently, hMSCs of modified volume (100 μL) were injected (Figure 5a). For the “L (Fastened)” group, a permanent magnet was fixed at the abdomen side (underneath the substrate) of the mice. We verified stem cell adhesion to the implanted substrates through the colocalization of human-specific HuNu- and DAPI-positive immunofluorescence-stained images in all of the injected hMSCs, which were independently pronounced in the “S” and the “L (Fastened)” groups. Thus, these two groups exhibited highly promoted stem cell adhesion with considerably elevated number of adhered stem cells and focal adhesions along with high nucleus/cytoplasm YAP and RUNX2 ratio and large spread cell area with low aspect ratio (Figure 5b,c; and Figure S24a,b, Supporting Information), which suggests that this activation of stem cell differentiation will facilitate tissue regeneration (Figure 5b,c). In contrast, pronounced stem cell adhesion, mechanotransduction, and differentiation

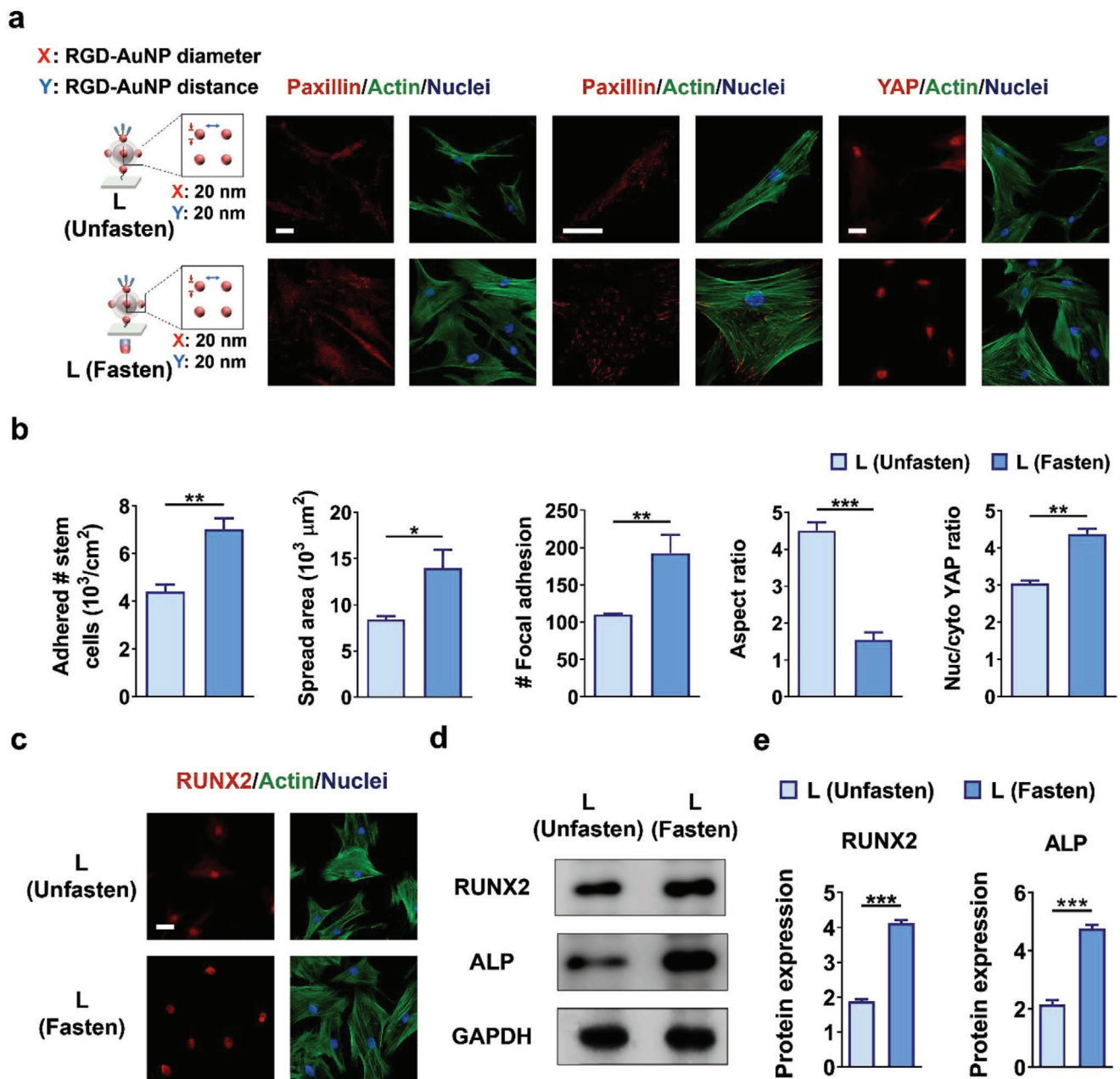


Figure 4. Magnetic fastening of the unconnected “L” group facilitates dynamic stem cell adhesion, mechanotransduction, and differentiation. a) Confocal microscopy images after immunofluorescence staining for paxillin and YAP costained with F-actin/nuclei after 48 h of culturing on the “L (Unfastened)” or “L (Fastened)” group in growth media and b) following quantifications of the number of adhered stem cells, spread cell area, the number of focal adhesions, cell aspect ratio, and nucleus/cytoplasm YAP ratio with the following notations: (RGD diameter, edge-to-edge RGD distance). A permanent magnet was placed at the lower side of the RGD-AuNP arrangements in the “L (Fastened)” group, which was not placed in the “L (Unfastened)” group. c) Confocal microscopy images after immunofluorescence staining for RUNX2 with F-actin/nuclei of stem cells and d) western blotting analysis for RUNX2 and ALP with e) corresponding protein expression quantification (normalized to GAPDH) after 4 d of culturing in osteogenic induction medium on the identical groups as above. Scale bars: 50 μm . Data are shown as the mean \pm standard error ($n = 10$). Asterisks were assigned to p values with statistical significances for multiple groups compared by one-way analysis of variance with Tukey–Kramer post-hoc tests (*: $p < 0.05$; **: $p < 0.01$; ***: $p < 0.001$). The experiments in a–e) were repeated three times.

were not observed in the “M” and “L (Unfastened)” groups. These findings collectively indicate that magnetically regulating the RGD fastening indeed stimulates integrin clustering on the unconnected RGDs and subsequent stem cell adhesion, mechanosensing, and differentiation in vivo similarly to the

quasi-connected RGDs. Along with the safe application of Fe_3O_4 materials and high magnetic fields to patients,^[36] the tunable RGD arrangements on Fe_3O_4 nanotemplates on the implanted substrates remained stable without any evidence of degradation, thereby suggesting the potential utility of the receptor-level

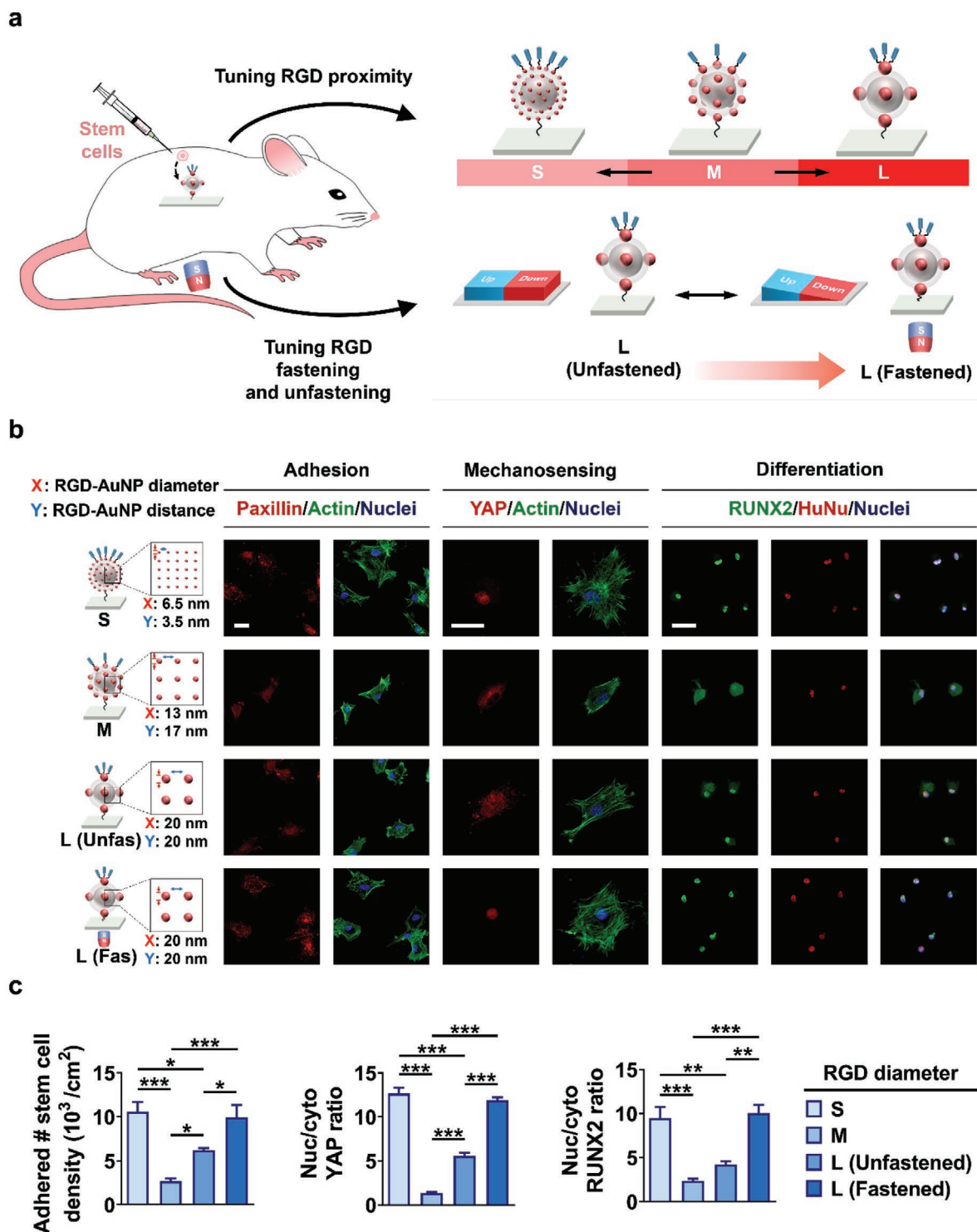


Figure 5. In vivo validation of quasiconnection and remote fastening of unconnected RGD arrangements independently activating stem cell adhesion, mechanosensing, and differentiation. a) A schematic representation of the tunable RGD-AuNP arrangements on Fe_3O_4 nanotemplates and their remote fastening on the substrates subcutaneously implanted into mice: “S,” “M,” “L (Unfastened),” and “L (Fastened)” groups with the following notations: (RGD diameter, edge-to-edge RGD distance). For the “L (Fastened)” group, a magnet was placed on the abdomen side of the mice, which was not placed in the “L (Unfastened)” (20, 20) group. b) Confocal microscopy images after immunofluorescence staining for paxillin and YAP costained with F-actin/nuclei, and early osteogenic marker (RUNX2) costained with human-specific nuclear antigen (HuNu) and nuclei in adhered stem cells (Scale bars: 50 μm) at 6 h postimplantation. c) Following quantification of the number of the adhered stem cells and the nucleus/cytoplasm YAP and RUNX2 ratio. Data are displayed as the mean \pm standard error ($n = 5$). Asterisks were assigned to p values with statistical significances for multiple groups compared by one-way analysis of variance with Tukey–Kramer post-hoc tests (*: $p < 0.05$; **: $p < 0.01$; ***: $p < 0.001$). The experiments in b,c) were repeated three times.

RGD proximity tuning for regulating stem cell-based tissue repair (Figure S25a,b, Supporting Information). Therefore, we confirmed the biomedical applicability of our material by analyzing stem cell differentiation, which provides evidence of the osteogenic differentiation and suggests potential long-term application that leads to bone tissue regeneration.

3. Conclusion

In summary, we independently tuned the RGD-bearing AuNP diameter and inter-distance at receptor-level proximity via seed-mediated growth of AuNPs on the Fe₃O₄ nano-templates, which are flexibly grafted to a substrate. We present “receptor-level RGD proximity” that efficiently regulates integrin clustering-mediated stem cell adhesion and differentiation both in vitro and in vivo. Robust cell adhesion is established when integrin binds to neighboring RGD sites within the level of integrin. When the RGD inter-distance exceeded the threshold of 17 nm (slightly exceeding the size of the FN and integrin), RGDs were considered to be unconnected by the stem cells, which significantly suppressed integrin binding between the neighboring RGD sites.

The RGD diameter exceeding a threshold of 20 nm slightly promoted multiple integrins binding to each 20 nm RGD site and partially to the neighboring RGDs, thereby stimulating integrin clustering, which leads to enhanced focal adhesion, mechanotransduction, and differentiation of stem cells. Remote manipulation of attracting the RGD arrangements towards the substrate by bending the polymer linker dynamically fastened the unconnected RGD arrangement, which significantly mediated stable integrin binding and clustering and thus augmented focal adhesion, mechanotransduction, and differentiation of stem cells to a degree comparable to the quasiconnected RGD arrangement. The molecular mechanisms for this effect involved actin polymerization, ROCK, and myosin II. As revealed via real-time confocal microscopy imaging, reversible stem cell adhesion was mediated by magnetically fastening and then unfastening the RGDs, which switched the RGD states from quasi-connected to unconnected states, respectively. The various conditions of seed-mediated AuNP growth on the nano-template to achieve various RGD diameter and inter-distance on diverse sizes and shapes of Fe₃O₄ nano-templates can help to elucidate the complex dynamic cell-nanogeometry interactions that will advance stem cell differentiation-mediated tissue repair.

Supporting Information

Supporting Information is available from the Wiley Online Library or from the author.

Acknowledgements

G.B. and M.S.K. contributed equally to this work. This work was supported by the National Research Foundation of Korea (NRF) grant funded by the Korean government (MSIT) (Nos. 2020R1C1C1011038 and 2019R1A2C3006587). This work was also supported by a Korea University Grant. HAADF-STEM imaging was conducted with the support of the Seoul center in Korea Basic Science Institute (KBSI). The surgery was

conducted after being approved by the Institutional Animal Care and Use Committee of Korea University.

Conflict of Interest

The authors declare no conflict of interest.

Data Availability Statement

The data that support the findings of this study are available in the supplementary material of this article.

Keywords

integrin clustering, ligand fastening, ligand proximity, stem cell adhesion, stem cell differentiation

Received: January 20, 2022

Revised: March 4, 2022

Published online:

- [1] a) J. K. Mouw, G. Q. Ou, V. M. Weaver, *Nat. Rev. Mol. Cell Biol.* **2014**, *15*, 771; b) E. Ruoslahti, M. D. Pierschbacher, *Science* **1987**, *238*, 491.
- [2] a) G. A. Di Lullo, S. M. Sweeney, J. Korkko, L. Ala-Kokko, J. D. San Antonio, *J. Biol. Chem.* **2002**, *277*, 4223; b) S. W. Chang, M. J. Buehler, *Mater. Today* **2014**, *17*, 70.
- [3] J. Engel, E. Odermatt, A. Engel, J. A. Madri, H. Furthmayr, H. Rohde, R. Timpl, *J. Mol. Biol.* **1981**, *150*, 97.
- [4] a) V. E. Koteliansky, M. A. Glukhova, M. V. Bejanian, V. N. Smirnov, V. V. Filimonov, O. M. Zalite, S. Y. Venyaminov, *Eur. J. Biochem.* **1981**, *119*, 619; b) V. Vogel, W. E. Thomas, D. W. Craig, A. Krammer, G. Baneyx, *Trends Biotechnol.* **2001**, *19*, 416; c) A. Krammer, D. Craig, W. E. Thomas, K. Schulten, V. Vogel, *Matrix Biol.* **2002**, *21*, 139.
- [5] Y. Jin, E. J. Jeon, S. Jeong, S. Min, Y. S. Choi, S. H. Kim, J. S. Lee, J. Shin, J. H. Yu, D. H. Ahn, Y.-G. Kim, H. S. Yang, T. J. Kang, S.-R. Cho, N. Choi, S.-W. Cho, *Adv. Funct. Mater.* **2021**, *31*, 2006227.
- [6] J. P. Xiong, T. Stehle, R. G. Zhang, A. Joachimiak, M. Frech, S. L. Goodman, M. A. Arnaout, *Science* **2002**, *296*, 151.
- [7] a) H. Kim, B. Kang, X. Cui, S. H. Lee, K. Lee, D. W. Cho, W. Hwang, T. B. Woodfield, K. S. Lim, J. Jang, *Adv. Funct. Mater.* **2021**, *31*, 2011252; b) Y. Ma, T. Han, Q. Yang, J. Wang, B. Feng, Y. Jia, Z. Wei, F. Xu, *Adv. Funct. Mater.* **2021**, *31*, 2100848.
- [8] R. Glazier, J. M. Brockman, E. Bartle, A. L. Mattheyses, O. Destaing, K. Salaita, *Nat. Commun.* **2019**, *10*, 4507.
- [9] a) F. Gonzalez-Perez, J. Hernandez, C. Heimann, J. B. Phillips, E. Udina, X. Navarro, *J. Neurosurg-Spine* **2018**, *28*, 109; b) L. R. Giam, M. D. Massich, L. Hao, L. S. Wong, C. C. Mader, C. A. Mirkin, *Proc. Natl. Acad. Sci. USA* **2012**, *109*, 4377; c) A. Y. Clark, K. E. Martin, J. R. García, C. T. Johnson, H. S. Theriault, W. M. Han, D. W. Zhou, E. A. Botchwey, A. J. García, *Nat. Commun.* **2020**, *11*, 114; d) J. Du, Y. Yao, M. Wang, R. Su, X. Li, J. Yu, B. Ding, *Adv. Funct. Mater.* **2021**, *32*, 2109833.
- [10] C. J. Flaim, S. Chien, S. N. Bhatia, *Nat. Methods* **2005**, *2*, 119.
- [11] B. Trappmann, J. E. Gautrot, J. T. Connelly, D. G. T. Strange, Y. Li, M. L. Oyen, M. A. C. Stuart, H. Boehm, B. J. Li, V. Vogel, J. P. Spatz, F. M. Watt, W. T. S. Huck, *Nat. Mater.* **2012**, *11*, 642.
- [12] A. E. Stanton, X. M. Tong, F. Yang, *Acta Biomater.* **2019**, *96*, 310.
- [13] Q. Li, G. Qi, X. Liu, J. Bai, J. Zhao, G. Tang, Y. S. Zhang, R. Chen-Tsai, M. Zhang, D. Wang, *Adv. Funct. Mater.* **2021**, *31*, 2104046.

- [14] a) A. K. Gaharwar, I. Singh, A. Khademhosseini, *Nat. Rev. Mater.* **2020**, *5*, 686; b) K. Lee, Y. Xue, J. Lee, H. J. Kim, Y. Liu, P. Tebon, E. Sarikhani, W. Sun, S. Zhang, R. Haghniaz, Ç.-S. Betül, X. Zhou, O. Serge, A. Samad, A. Nureddin, M. R. D, A. Khademhosseini, *Adv. Funct. Mater.* **2020**, *30*, 2000086; c) T. Hoffman, P. Antovski, P. Tebon, C. Xu, N. Ashammakhi, S. Ahadian, L. Morsut, A. Khademhosseini, *Adv. Funct. Mater.* **2020**, *30*, 1909882; d) W. Li, W. Miao, Y. Liu, T. Wang, Y. Zhang, W. Wang, D. Lu, X. Zhou, X. Jiao, X. Jia, *Adv. Funct. Mater.* **2021**, *32*, 2109871.
- [15] a) K. H. Vining, D. J. Mooney, *Nat. Rev. Mol. Cell Biol.* **2017**, *18*, 728; b) O. Rossier, V. Octeau, J. B. Sibarita, C. Leduc, B. Tessier, D. Nair, V. Gatterdam, O. Destaing, C. Albiges-Rizo, R. Tampe, L. Cognet, D. Choquet, B. Lounis, G. Giannone, *Nat. Cell Biol.* **2012**, *14*, 1057.
- [16] a) E. A. Cavalcanti-Adam, A. Micoulet, J. Blummel, J. Auernheimer, H. Kessler, J. P. Spatz, *Eur. J. Cell Biol.* **2006**, *85*, 219; b) E. A. Cavalcanti-Adam, T. Volberg, A. Micoulet, H. Kessler, B. Geiger, J. P. Spatz, *Biophys. J.* **2007**, *92*, 2964.
- [17] M. Schwartzman, M. Palma, J. Sable, J. Abramson, X. A. Hu, M. P. Sheetz, S. J. Wind, *Nano Lett.* **2011**, *11*, 1306.
- [18] a) C. S. Chen, M. Mrksich, S. Huang, G. M. Whitesides, D. E. Ingber, *Science* **1997**, *276*, 1425; b) X. Wang, S. Y. Li, C. Yan, P. Liu, J. D. Ding, *Nano Lett.* **2015**, *15*, 1457.
- [19] J. H. Huang, S. V. Grater, F. Corbellini, S. Rinck, E. Bock, R. Kemkemer, H. Kessler, J. D. Ding, J. P. Spatz, *Nano Lett.* **2009**, *9*, 1111.
- [20] J. A. Deeg, I. Louban, D. Aydin, C. Selhuber-Unkel, H. Kessler, J. P. Spatz, *Nano Lett.* **2011**, *11*, 1469.
- [21] L. Y. Koo, D. J. Irvine, A. M. Mayes, D. A. Lauffenburger, L. G. Griffith, *J. Cell Sci.* **2002**, *115*, 1423.
- [22] S. Min, Y. S. Jeon, H. J. Jung, C. Khatua, N. Li, G. Bae, H. Choi, H. Hong, J. E. Shin, M. J. Ko, H. S. Ko, I. Jun, H. E. Fu, S. H. Kim, R. Thangam, J. J. Song, V. P. Dravid, Y. K. Kim, H. Kang, *Adv. Mater.* **2020**, *32*, 2004300.
- [23] R. Changede, H. G. Cai, S. J. Wind, M. P. Sheetz, *Nat. Mater.* **2019**, *18*, 1366.
- [24] Z. Liu, O. L. Lanier, A. Chauhan, *Nanomaterials* **2020**, *10*, 2359.
- [25] Y. Jin, J. S. Lee, J. Kim, S. Min, S. Wi, J. H. Yu, G. E. Chang, A. N. Cho, Y. Choi, D. H. Ahns, S. R. Cho, E. Cheong, Y. G. Kim, H. P. Kim, Y. Kim, D. S. Kim, H. W. Kim, Z. Quan, H. C. Kang, S. W. Cho, *Nat. Biomed. Eng.* **2018**, *2*, 522.
- [26] a) B. S. Gomes, B. Simões, P. M. Mendes, *Nat. Rev. Chem.* **2018**, *2*, 0120; b) Y. Kim, H. Choi, J. E. Shin, G. Bae, R. Thangam, H. Kang, *View* **2020**, *1*, 20200029; c) W. Li, Z. Yan, J. Ren, X. Qu, *Chem. Soc. Rev.* **2018**, *47*, 8639; d) T. T. Lee, J. R. Garcia, J. I. Paez, A. Singh, E. A. Phelps, S. Weis, Z. Shafiq, A. Shekaran, A. del Campo, A. J. Garcia, *Nat. Mater.* **2015**, *14*, 352; e) F. Gong, L. Cheng, N. Yang, Y. Gong, Y. Ni, S. Bai, X. Wang, M. Chen, Q. Chen, Z. Liu, *Nat. Commun.* **2020**, *11*, 3712; f) H. Luo, L. Kong, F. Zhang, C. Huang, J. Chen, H. Zhang, H. Yu, S. Zheng, H. Xu, Y. Zhang, *Adv. Funct. Mater.* **2021**, *31*, 2101262; g) S. Pearson, J. Feng, A. del Campo, *Adv. Funct. Mater.* **2021**, *31*, 2105989.
- [27] a) J. U. Lee, W. Shin, Y. Lim, J. Kim, W. R. Kim, H. Kim, J. H. Lee, J. Cheon, *Nat. Mater.* **2021**, *20*, 1029; b) B. Yu, B. S. Choi, W. G. Li, D. H. Kim, *Nat. Commun.* **2020**, *11*, 3637.
- [28] a) J. Hong, M. Kang, M. Jung, Y. Y. Lee, Y. Cho, C. Kim, S. Y. Song, C. G. Park, J. Doh, B. S. Kim, *Adv. Mater.* **2021**, *33*, 2101110; b) W. Baek, M. S. Bootharaju, S. Lorenz, S. Lee, S. Stolte, R. Fainblat, G. Bacher, T. Hyeon, *Adv. Funct. Mater.* **2021**, *31*, 2107447; c) R. Fu, H. Li, R. Li, K. McGrath, G. Dotti, Z. Gu, *Adv. Funct. Mater.* **2021**, *31*, 2009489; d) V. Bhingardive, A. Edri, A. Kossover, G. L. Saux, B. Khand, O. Radinsky, M. Iraqi, A. Porgador, M. Schwartzman, *Adv. Funct. Mater.* **2021**, *31*, 2103063; e) J. Huang, B. Yang, Y. Peng, J. Huang, S. H. D. Wong, L. Bian, K. Zhu, X. Shuai, S. Han, *Adv. Funct. Mater.* **2021**, *31*, 2011171; f) S. H. D. Wong, X. Xu, X. Chen, Y. Xin, L. M. Xu, C. H. N. Lai, J. Oh, W. K. R. Wong, X. M. Wang, S. S. Han, W. X. You, X. T. Shuai, N. Wong, Y. H. Tan, L. Duan, L. M. Bian, *Nano Lett.* **2021**, *21*, 3225; g) S. H. D. Wong, J. N. Li, X. H. Yan, B. Wang, R. Li, L. Zhang, L. M. Bian, *Nano Lett.* **2017**, *17*, 1685; h) S. H. D. Wong, W. K. R. Wong, C. H. N. Lai, J. Oh, Z. Li, X. Y. Chen, W. H. Yuan, L. M. Bian, *Nano Lett.* **2020**, *20*, 3207.
- [29] a) T. Wiegand, M. Fratini, F. Frey, K. Yserentant, Y. Liu, E. Weber, K. Galior, J. Ohmes, F. Braun, D.-P. Herten, *Nat. Commun.* **2020**, *11*, 32; b) W. Baek, M. S. Bootharaju, K. M. Walsh, S. Lee, D. R. Gamelin, T. Hyeon, *Nat. Mater.* **2021**, *20*, 650; c) J. Mao, L. Chen, Z. Cai, S. Qian, Z. Liu, B. Zhao, Y. Zhang, X. Sun, W. Cui, *Adv. Funct. Mater.* **2021**, *32*, 2111003.
- [30] a) M. J. Dalby, N. Gadegaard, R. O. Oreffo, *Nat. Mater.* **2014**, *13*, 558; b) K. S. Kim, J. Y. Lee, J. Han, H. S. Hwang, J. Lee, K. Na, *Adv. Funct. Mater.* **2019**, *29*, 1900773; c) X. Wan, Z. Liu, L. Li, *Adv. Funct. Mater.* **2021**, *31*, 2010626.
- [31] a) S. Min, M. J. Ko, H. J. Jung, W. Kim, S. B. Han, Y. Kim, G. Bae, S. Lee, R. Thangam, H. Choi, N. Li, J. E. Shin, Y. S. Jeon, H. S. Park, Y. J. Kim, U. K. Sukumar, J. J. Song, S. K. Park, S. H. Yu, Y. C. Kang, K. B. Lee, Q. Wei, D. H. Kim, S. M. Han, R. Paulmurugan, Y. K. Kim, H. Kang, *Adv. Mater.* **2021**, *33*, 2008353; b) G. Bae, Y. S. Jeon, M. J. Ko, Y. Kim, S. B. Han, R. Thangam, W. Kim, H. J. Jung, S. Lee, H. Choi, S. Min, H. Hong, S. Park, S. Y. Kim, K. D. Patel, N. Li, J. E. Shin, B. C. Park, H. S. Park, J. H. Moon, Y. J. Kim, U. K. Sukumar, J. J. Song, S. Y. Kim, S. H. Yu, Y. C. Kang, S. Park, S. M. Han, D. H. Kim, K. B. Lee, et al., *Adv. Funct. Mater.* **2021**, *31*, 2103409.
- [32] H. Choi, G. Bae, C. Khatua, S. Min, H. J. Jung, N. Li, I. Jun, H. W. Liu, Y. Cho, K. H. Na, M. Ko, H. Shin, Y. H. Kim, S. Chung, J. J. Song, V. P. Dravid, H. Kang, *Adv. Funct. Mater.* **2020**, *30*, 2001446.
- [33] a) X. Xue, Y. Hu, Y. Deng, J. Su, *Adv. Funct. Mater.* **2021**, *31*, 2009432; b) P. Kumar, K. B. Mirza, K. Choudhury, M. Cucchiari, H. Madry, P. Shukla, *Adv. Funct. Mater.* **2021**, *31*, 2009663.
- [34] T. C. von Erlach, S. Bertazzo, M. A. Wozniak, C. M. Horejs, S. A. Maynard, S. Attwood, B. K. Robinson, H. Autefage, C. Kallepitis, A. D. Hernandez, C. S. Chen, S. Goldoni, M. M. Stevens, *Nat. Mater.* **2018**, *17*, 237.
- [35] S. J. Attwood, E. Cortes, A. W. M. Haining, B. Robinson, D. Li, J. Gautrot, A. del Río Hernández, *Sci. Rep.* **2016**, *6*, 34334.
- [36] a) K. Maier-Hauff, F. Ulrich, D. Nestler, H. Niehoff, P. Wust, B. Thiesen, H. Orawa, V. Budach, A. Jordan, *J. Neurooncol.* **2011**, *103*, 317; b) M. Prothmann, F. von Knobelsdorff-Brenkenhoff, A. Topper, M. A. Dieringer, E. Shahid, A. Graessl, J. Rieger, D. Lysiak, C. Thalhammer, T. Huelnhagen, P. Kellman, T. Niendorf, J. Schulz-Menger, *PLoS One* **2016**, *11*, e0148066.